

Absence of a critical nematic phase in the vicinity of the SU(3) ferromagnetic point for the one-dimensional spin-1 bilinear-biquadratic model

Yan-Wei Dai,¹ Qian-Qian Shi,¹ Huan-Qiang Zhou,¹ and Ian McCulloch²

¹Centre for Modern Physics, Chongqing University, Chongqing 400044, The People's Republic of China

²School of Mathematics and Physics, The University of Queensland, St. Lucia, QLD 4072, Australia

The absence of a critical nematic phase in the vicinity of the SU(3) ferromagnetic point for the one-dimensional spin-1 bilinear-biquadratic model is demonstrated by means of the tensor network algorithms. As it turns out, the phase transition from the ferromagnetic phase to the dimerized phase at the SU(3) ferromagnetic point is direct, but not of the first-order. The transition point features highly degenerate ground states, which are scale but not conformally invariant, with the fractal dimension being equal to 2. The conceptual developments in effective field theories - the fractal dimension and the counting rule of the Goldstone modes - play a pivotal role in clarifying the numerical artifacts arising from the finiteness of the bond dimension in the tensor network simulations, which are attributed to a proximity effect to a highly entangled scale or conformally invariant ground state.

PACS numbers:

Introduction.- The spin-1 bilinear-biquadratic model has been investigated extensively, either analytically or numerically [1–12]. It is described by the Hamiltonian with the nearest-neighbor interactions

$$H = \sum_j \left[\cos \phi (\mathbf{S}_j \mathbf{S}_{j+1}) + \sin \phi (\mathbf{S}_j \mathbf{S}_{j+1})^2 \right], \quad (1)$$

where $\mathbf{S}_j = (S_j^x, S_j^y, S_j^z)$ denote the spin-1 operators acting on the j -th site. The model exhibits rich physics, with the ground-state phase diagram being shown in Fig. 1. A remarkable example is the Haldane gap in the spin-1 Heisenberg antiferromagnet [13] at $\phi = 0$, which is adiabatically connected to the Affleck-Kennedy-Lieb-Tasaki point at $\phi = \arctan(1/3)$ [14], with its ground state being the valence-bond-solid state. This exactly solved point provides compelling evidence for the existence of the gapped Haldane phase with hidden topological order [13, 15] for $-\pi/4 < \phi < \pi/4$. The importance of the model (1) is also embodied in the fact that it is exactly solvable by means of the Bethe ansatz at a few selected points, including $\phi = \pi/4$ [16], $\phi = -\pi/2$ [17], and $\phi = -\pi/4$ [18]. In addition, the model exhibits the SU(3) symmetry [19–21] at $\phi = \pm\pi/2, \pi/4$, and $-3\pi/4$ (cf. also Sec. SI in the Supplementary Material (SM) [22]). However, whether or not the phase transition from the ferromagnetic phase to the dimerized phase is direct remains to be controversial up to present.

The controversy dates back to a pioneering work by Chubukov [1], who suggested that a gapped nematic phase exists between the dimerized phase and the ferromagnetic phase. In contrast, Fath and Solyom [2] advocated that the phase transition from the ferromagnetic phase to the dimerized phase is direct and of the first-order, thus ruling out the existence of the gapped nematic phase. They also argued that an exponentially decaying small gap opens once away from the SU(3) ferromagnetic point. However, no mechanism is offered to account for the opening of such an exponentially decaying small gap. Subsequently, an extensive investigation has been done [3–10], in attempt to settle this controversial

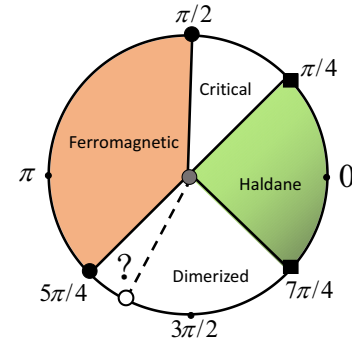


FIG. 1: (color online) A sketch of the ground state phase diagram for the one-dimensional spin-1 bilinear-biquadratic model. Here, ϕ ranges from 0 to 2π , but we focus on a region in the vicinity of the SU(3) ferromagnetic point at $\phi = 5/4\pi$. The question mark indicates a possible critical nematic phase, which turns out to be absent.

issue. Buchta *et al* [5] showed that the dimerized phase prevails down to the SU(3) point, although a non-dimerized phase is possible in a narrow range close to the SU(3) ferromagnetic point. In Refs. [7, 10], a critical nematic phase is suggested as a possible non-dimerized phase between the ferromagnetic phase and the dimerized phase. Meanwhile, Rizzi *et al* [6] concluded that there is no intermediate nematic phase, but a tendency is enhanced towards the nematic order. Instead, Lachli, Schmid, and Trebst [7] suggested that an unconventional crossover might lie at the heart of the complications concerning the presence or absence of a critical nematic phase. In a recent work [10], the SU(2) symmetry is implemented in a finite-size matrix product state (MPS) algorithm under the periodic boundary conditions, which is sufficient to confirm the absence of a critical nematic phase for $\phi/\pi > -0.72$, but leaving it open the possibility for the existence of a critical nematic phase in the vicinity of the SU(3) ferromagnetic point.

In this work, we adopt a completely different strategy to address this controversy. In our opinion, the current state-of-

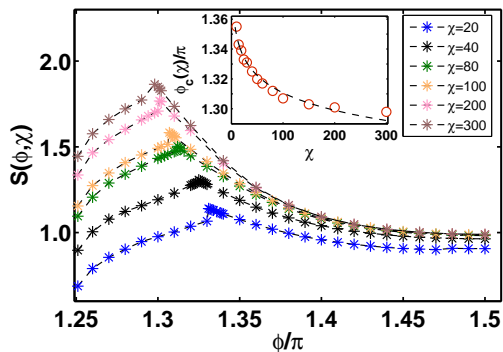


FIG. 2: (color online) Main: the entanglement entropy $S(\phi, \chi)$ as a function of ϕ , with the bond dimension $\chi = 20, 40, 80, 100, 200$ and 300 , from the iTEBD simulation. One pseudo critical point $\phi_c(\chi)$ is detected as a peak for each value of the bond dimension χ . Inset: an extrapolation of the pseudo critical points $\phi_c(\chi)$ is performed, as the bond dimension χ tends to infinity. Here, the termination point is chosen to be at the SU(3) ferromagnetic point. Thus, the data is fitted in the form: $\phi_c(\chi) = 5/4\pi + p\chi^q$, where $p = -2.54$ and $q = -0.0064$.

the-art algorithms in the context of the tensor network representations are powerful enough to efficiently simulate the model (1), including the infinite time evolving block decimation (iTEBD) [23], the U(1) infinite density matrix renormalization group (iDMRG) algorithm, and the SU(2) iDMRG algorithm [24]. For our purpose, we focus on the region $5\pi/4 < \phi < 3\pi/2$. As it turns out, different types of numerical artifacts arise from the finiteness of the bond dimension in the tensor network simulations, if different symmetries are implemented. The artifacts may be characterized in terms of the fractal dimension [25] and the counting rule of the Goldstone modes (GMs) [26] - recent conceptual developments in effective field theories. As a consequence, there are two distinct types of the artifacts, which may be attributed to a proximity effect to two types of highly entangled ground states: one is conformally invariant and the other is scale invariant, thus leading to a pseudo critical regime and a pseudo fractal regime. Here, by “pseudo” we mean an artifact arising from the finiteness of the bond dimension in the tensor network simulations. It is the presence of the numerical artifacts that makes it very hard to extract the underlying physics behind the model (1).

The iTEBD simulation.- The iTEBD simulation is performed in the region $(1.25\pi, 1.5\pi]$. In Fig. 2, the entanglement entropy $S(\phi, \chi)$, which quantifies the entanglement of a bipartite system [27], is plotted as a function of ϕ , with the bond dimension $\chi = 20, 40, 80, 100, 200$ and 300 . Here, we note that in the infinite MPS representation, the entanglement entropy $S(\phi, \chi)$ for the semi-infinite chain may be written as $S(\phi, \chi) = -\sum_{\mu} \lambda_{\mu}^2(\phi, \chi) \ln \lambda_{\mu}^2(\phi, \chi)$, with $\lambda_{\mu}^2(\phi, \chi)$ being the Schmidt decomposition coefficients. The entanglement entropy $S(\phi, \chi)$ exhibits a singular peak, with each singular point being indicative of a pseudo critical point $\phi_c(\chi)$. Hence, there is a pseudo critical point $\phi_c(\chi)$ for a given value of the bond dimension χ , separating the whole region into a pseudo critical

regime and a dimerized regime. As an illustrative example, for the bond dimension $\chi = 300$, the pseudo critical point $\phi_c(\chi)$ is located at $\phi_c(\chi) = 1.298\pi$.

In order to characterize the pseudo critical regime, we need to extract the central charge c from the finite-entanglement scaling [28, 29]:

$$S(\phi, \chi) = \frac{c}{6} \ln \xi(\phi, \chi) + a(\phi), \quad (2)$$

where $\xi(\phi, \chi) \propto \chi^{\kappa(\phi)}$, with $\kappa(\phi)$ being the finite entanglement scaling exponent, and $a(\phi)$ is an additive constant. The best linear fit is performed for $\phi = 1.26\pi, 1.27\pi, 1.28\pi$ and 1.29π , with the bond dimension ranging from 16 to 300, respectively. The central charge c is estimated to be $c = 2$, with a relative error being less than 2%, in the entire pseudo critical regime (for details, see Sec. SII in SM [22]). Meanwhile, the central charge c is also extracted from the pseudo critical points $\phi_c(\chi)$, yielding $c = 1.86$, with a relative error being less than 7%, compared to the expected exact value $c = 2$ (cf. Sec. SII in SM [22]). We attribute a higher relative error in this case to the fact that the accuracies of the pseudo critical points $\phi_c(\chi)$ are relatively lower, due to high computational costs.

Physically, the fact that the central charge $c = 2$ in the pseudo critical regime may be explained in terms of the counting rule of the (pseudo) GMs adapted to numerical artifacts. Actually, this arises from the pseudo spontaneous symmetry breaking (SSB) [30] from SU(2) to U(1), in which two generators are spontaneously broken, thus resulting in two pseudo GMs of type-A, with the central charge c being the number of the pseudo GMs, given that the central charge c measures the number of the gapless excitations [31]. Here, we note that the infinite MPS algorithm naturally leads to infinitely degenerate ground states in a pseudo critical regime, due to the finiteness of the bond dimension. In fact, if the bond dimension χ tends to infinity, then a pseudo local order parameter $\langle O_j \rangle$ arising from pseudo SSB tends to vanish, as required to keep consistency with the Mermin-Wagner theorem [32]. In our case, the pseudo local order parameter $\langle O_j \rangle$ is defined as follows

$$\langle O_j \rangle = \sqrt{\sum_{\alpha, \beta=1}^8 g^{\alpha\beta} \langle K_{\alpha}^j \rangle \langle K_{\beta}^j \rangle}, \quad (3)$$

where $g^{\alpha\beta} = g_{\alpha\beta}^{-1}$, $g_{\alpha\beta}$ is a metric tensor: $g_{\alpha\beta} = \sum_{\delta, \epsilon} \gamma_{\alpha\delta\epsilon} \gamma_{\beta\delta\epsilon}$ ($\alpha, \beta, \delta, \epsilon = 1, 2, \dots, 8$), with $\gamma_{\alpha\beta\delta}$ being the structural constants of the SU(3) group, and K_{α}^j is the local components of the SU(3) generators at the j -th site. Since the iTEBD simulation is performed for a randomly chosen initial state, it yields a ground state wave function in the infinite MPS representation, with different expectation values of the generators K_{α}^j . However, the pseudo local order operator $\langle O_j \rangle$ does not depend on an initial state, within accuracies. It is found that the same set of the pseudo critical points $\phi_c(\chi)$ are detected in terms of the pseudo local order parameter $\langle O_j(\chi) \rangle$, consistent with those from the entanglement entropy $S(\phi, \chi)$ and the pseudo local order parameter $\langle O_j(\chi) \rangle$ is scaled down to zero (for details, cf. Sec. SIV in SM [22]).

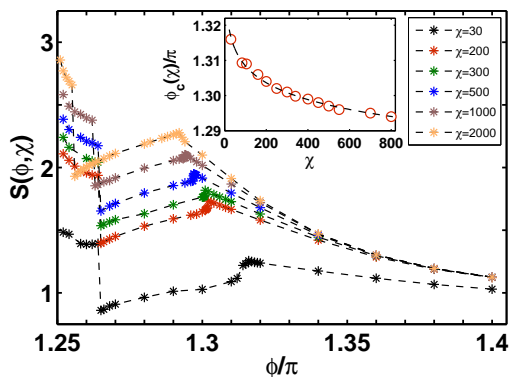


FIG. 3: (color online) Main: the entanglement entropy $S(\phi, \chi)$ as a function of ϕ , with the bond dimension $\chi = 30, 200, 300, 500, 1000$ and 2000 , from the U(1) iDMRG simulation. One pseudo first-order transition point $\phi_f(\chi)$ and one pseudo critical point $\phi_c(\chi)$ are detected as a (discontinuous) dip and a peak for each value of the bond dimension χ , respectively. Inset: an extrapolation of the pseudo critical points $\phi_c(\chi)$ is performed, as the bond dimension χ tends to infinity, assuming $\phi_c(\chi)$ terminate at the SU(3) ferromagnetic point. Thus, the data is fitted in the form: $\phi_c(\chi) = 5/4\pi + p\chi^q$, where $p = -2.587$ and $q = -0.0026$.

In addition, the dimerized phase is characterized in terms of the local order parameter $\langle D_{j,j+1} \rangle = \langle \mathbf{S}_j \mathbf{S}_{j+1} - \mathbf{S}_{j+1} \mathbf{S}_{j+2} \rangle$, which tends to be saturated as the bond dimension χ increases.

A crucial question concerns whether or not the pseudo critical points $\phi_c(\chi)$ terminate at the SU(3) ferromagnetic point, if the bond dimension χ tends to infinity. As shown in Fig. 2, it is possible for the pseudo critical points $\phi_c(\chi)$ to terminate at the SU(3) ferromagnetic point. Here, the termination point is chosen to be at the SU(3) ferromagnetic point. Thus, the fitting function takes the form: $\phi_c(\chi) = 5/4\pi + p\chi^q$, where $p = -2.54$ and $q = -0.0064$. However, such an extrapolation also works within the accuracies, if we make any other choice of the termination point, as long as it is close enough to the SU(3) ferromagnetic point. As a consequence, two possible scenarios arise: (i) the pseudo critical points $\phi_c(\chi)$ terminate at the SU(3) ferromagnetic point, when the bond dimension χ tends to infinity; (ii) the pseudo critical points $\phi_c(\chi)$ terminate at a point ϕ_c away from the SU(3) ferromagnetic point, when the bond dimension χ tends to infinity. In the first scenario, there is no critical nematic phase between the SU(3) ferromagnetic point and the dimerized phases. In the second scenario, there is a critical nematic phase between the SU(3) ferromagnetic point and the dimerized phases, with the central charge c being 2 (for details, cf Sec. SVI in SM [22]).

The U(1) iDMRG simulation. - The U(1) iDMRG algorithm with two-site translational invariance, is exploited, targeting at a ground state, with the z -component of the total spin being zero, to simulate the model (1) in the same region. In Fig. 3, we plot the entanglement entropy $S(\phi, \chi)$ as a function of ϕ , with the bond dimension $\chi = 30, 200, 300, 500, 1000$ and 2000 . It is found that a peak and a (discontinuous) dip appear, indicating that there are two pseudo phase transition points:

one is a pseudo critical point $\phi_c(\chi)$, consistent with the iTEBD simulation, and the other is a pseudo first-order phase transition point $\phi_f(\chi)$, for each value of χ . The latter separates a pseudo critical regime with central charge $c = 2$ from a pseudo fractal regime. As an illustrative example, for $\chi = 2000$, the pseudo first-order phase transition point $\phi_f(\chi)$ and the pseudo critical point $\phi_c(\chi)$ are located at $\phi_f(\chi) = 1.256\pi$ and $\phi_c(\chi) = 1.292\pi$, respectively. We also perform an extrapolation of the pseudo critical points $\phi_c(\chi)$, as the bond dimension χ tends to infinity, assuming that the pseudo critical points $\phi_c(\chi)$ terminate at the SU(3) ferromagnetic point. Thus, the fitting function takes the form: $\phi_c(\chi) = 5/4\pi + p\chi^q$, where $p = -2.587$ and $q = -0.0026$ [33], as shown in Fig. 3.

To characterize the pseudo fractal regime, we resort to the finite block-size scaling of the entanglement entropy $S(n)$. As it turns out, it scales logarithmically with the block size n [25]:

$$S(n) = \frac{d_f}{2} \ln n + b. \quad (4)$$

Here, d_f is the fractal dimension, and b is an additive constant. For three different values of ϕ : $\phi = 1.26\pi, 1.254\pi$ and 1.252π in the pseudo fractal regime, we perform the best linear fit, yielding that $d_f = 1$, with a relative error being less than 4%, consistent with a general statement that the fractal dimension d_f is equal to the number of the (pseudo) GMs of type-B [34](also cf. Sec. SVII in SM [22]).

From the finite-entanglement scaling (2), the central charge c is extracted for $\phi = 1.26\pi, 1.27\pi, 1.28\pi$ and 1.29π in the pseudo critical regime, yielding $c = 2$, with a relative error being less than 4%. This is in agreement with that from the iTEBD simulation. Meanwhile, the central charge c is extracted from a pseudo critical point $\phi_c(\chi)$ between the pseudo critical regime and the dimerized regime, which yields $c = 1.833$, with a relative error being less than 8.4%, compared to the exact value $c = 2$.

Both the pseudo fractal regime and the pseudo critical regime may be characterized in terms of the pseudo order parameter $\langle O_j \rangle$. From the U(1) iDMRG simulation, one finds that only $K_4^j = I - 3/2\langle S_j^z \rangle^2$ yields a non-zero expectation value. Therefore, the pseudo local order parameter $\langle O_j \rangle$ may be replaced by $\langle \langle S_j^z \rangle^2 \rangle$. Hence, the pseudo first-order phase transition point $\phi_f(\chi)$ and the pseudo critical points $\phi_c(\chi)$ are determined from the pseudo local order parameter $\langle \langle S_j^z \rangle^2 \rangle$, consistent with those from the entanglement entropy $S(\phi, \chi)$. We stress that the two regimes may be distinguished by means of the pseudo local order parameter $\langle \langle S_j^z \rangle^2 \rangle$, with pseudo SSB from SU(2) to U(1) in two distinct ways. In the pseudo fractal regime, we have $\langle \langle S_j^z \rangle^2 \rangle > 2/3$: SU(2) is spontaneously broken to U(1), with two broken generators corresponding to one pseudo GM of type-B. In contrast, in the pseudo critical regime, we have $\langle \langle S_j^z \rangle^2 \rangle < 2/3$: SU(2) is spontaneously broken to U(1), with two broken generators corresponding to two pseudo GMs of type-A. Note that $\langle \langle S_j^z \rangle^2 \rangle$ approaches 2/3 to recover the SU(2) invariance, as the bond dimension χ goes to infinity.

The presence of the pseudo first-order phase transition

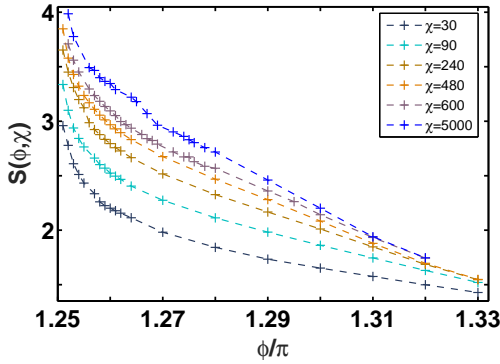


FIG. 4: The entanglement entropy $S(\phi, \chi)$ as a function of ϕ , with the bond dimension $\chi = 30, 90, 240, 480, 600$ and 5000 , from the SU(2) iDMRG simulation. Note that no phase transition is detected in the region $(1.262\pi, 1.33\pi]$, in which the simulation results are reliable.

points $\phi_f(\chi)$ from the U(1) iDMRG simulation makes it possible to refine the two scenarios from the iTEBD. In particular, this entails an important implication for the second scenario. Suppose the pseudo critical points $\phi_c(\chi)$ terminate at a critical point ϕ_c , as the bond dimension χ tends to infinity. Then, the critical point ϕ_c must be located at a value of ϕ greater than ϕ_o . Here, ϕ_o denotes an onset point where the pseudo fractal regime sets in, which reflects ferromagnetic fluctuations from the SU(3) ferromagnetic point. Physically, this amounts to stating that the pseudo fractal regime is not allowed to extend to a point beyond the critical point ϕ_c , if it exists. For the first scenario, both $\phi_f(\chi)$ and $\phi_c(\chi)$ approach the SU(3) ferromagnetic point, as the bond dimension χ tends to infinity.

The SU(2) iDMRG simulation.- We exploit the SU(2) iDMRG algorithm to simulate the model (1) in the region $(1.251\pi, 1.33\pi]$. In Fig.4, we plot the entanglement entropy $S(\phi, \chi)$ as a function of ϕ , with the bond dimension $\chi = 30, 90, 240, 480, 600$ and 5000 . The entanglement entropy $S(\phi, \chi)$ monotonically increases, as the bond dimension χ increases. Hence, the entanglement entropy $S(\phi, \chi)$ is smooth in the region $\phi \in (1.251\pi, 1.33\pi]$, indicating that no phase transition occurs. This observation is confirmed from the behaviors of the dimerized order parameter $\langle D_{j,j+1} \rangle$ and the ground state fidelity $d(\phi_1, \phi_2)$ per lattice site [35] (cf. SV in SM [22]).

Therefore, we are led to the conclusion that the second scenario is unlikely to be valid. That is, the dimerized phase is extended up to the SU(3) ferromagnetic point, and the phase transition from the ferromagnetic phase to the dimerized phase is direct, consistent with Ref. [2].

One might speculate that the simulation results from the SU(2) iDMRG algorithm alone are sufficient to rule out the possibility for the existence of the critical nematic phase. However, this is not the case, simply because the accuracies become worse, as the SU(3) ferromagnetic point is approached. Actually, it is the occurrence of the pseudo fractal regime in the U(1) iDMRG simulation that makes it unnecessary to get close to the SU(3) ferromagnetic point. Indeed, the simulation results from the SU(2) iDMRG algorithm are less

reliable when ϕ is in the region $(1.251\pi, 1.262\pi]$. However, the pseudo fractal regime in the U(1) iDMRG simulation extends at least up to 1.265π . That means ϕ_o is at least 1.265π . This in turn explains why it is sufficient to rule out the existence of a critical nematic phase, if no phase transition is detected in the region $(1.262\pi, 1.33\pi]$.

The origins of the pseudo fractal and critical regimes in the tensor network simulations.- The pseudo fractal regime only occurs in the U(1) iDMRG simulation. To unveil the origin of the pseudo fractal regime, we need first to clarify the underlying physics behind the SU(3) ferromagnetic model. Indeed, the ground states are scale but not conformally invariant [34]. In fact, two GMs of type-B emerge, as a consequence of SSB from SU(3) to SU(2) \otimes U(1), implying that the fractal dimension d_f is equal to 2, since the fractal dimension d_f measures the number of low-lying excitations (cf. SVII in SM [22]). Given a ground state with the z -component of the total spin being zero is targeted during the U(1) iDMRG simulation, one may attribute the pseudo fractal regime to a proximity effect to highly degenerate and highly entangled ground states at the SU(3) ferromagnetic point. On the other hand, the fractal dimension d_f is equal to 1 in the pseudo fractal regime, since one pseudo GM of type-B is present, as a result of pseudo SSB from SU(2) to U(1). Meanwhile, the pseudo GM of type-B smoothly evolves into one of the two GMs of type-B at the SU(3) ferromagnetic point.

The remaining question concerns what acts as the origin of the pseudo critical regime. In Ref. [36], the spin-1 bilinear-biquadratic model undergoing a quadratic Zeeman effect is unveiled to exhibit the KT transitions between the XY nematic phase and the dimerized phase. That is, there is a critical nematic phase with $c = 1$, which is infinitesimally close to the SU(3) ferromagnetic point. Therefore, if an extra term $D_x \sum_j (S_j^x)^2 + D_y \sum_j (S_j^y)^2 + D_z \sum_j (S_j^z)^2$ is included in the Hamiltonian (1), with D_x , D_y , and D_z being some coupling constants, one may expect that there are two critical nematic phases with $c = 1$, which extend up to the SU(3) ferromagnetic point, due to the local constraints $(S_j^x)^2 + (S_j^y)^2 + (S_j^z)^2 = 2$ (also cf. SVIII in SM [22]). As a consequence, two pseudo GMs of type-A emerge in the iTEBD and U(1) iDMRG simulations, as long as it is close enough to the SU(3) ferromagnetic point. In other words, it is the proximity effect to the two critical phases with $c = 1$ that constitutes the origin of the pseudo critical regime with $c = 2$ in the iTEBD and U(1) iDMRG simulations. However, the two critical phases with $c = 1$ do not meet each other at the SU(3) ferromagnetic point, though asymptotically close. This implies that no SU(2) WZW model with level $k = 4$ survives as a limit of the pseudo critical regime.

Concluding remarks.- We have performed extensive numerical simulations of the one-dimensional spin-1 bilinear-biquadratic model in the context of the tensor network algorithms. Our results demonstrate that different types of numerical artifacts arise from the tensor network algorithms, if different symmetries are implemented. There are two types of artifacts, attributed to a proximity effect to a highly entangled

ground state, either a conformally invariant critical regime or a scale invariant fractal regime. The artifacts may be characterized in terms of the fractal dimension [25] and the counting rule of the pseudo GMs [26].

A few closing remarks are in order. First, the suggestion made by Chubukov [1], though it has been ruled out, is not far from being true, in the sense that the two critical nematic phases with the central charge $c = 1$ are asymptotically close to the SU(3) ferromagnetic point, though no SU(2) WZW model at level $k = 4$ survives as a limit of the pseudo critical regime, as the bond dimension increases. It is the proximity effect to the two critical nematic phases that provides a mechanism responsible for the opening of an exponentially decaying small gap away from the SU(3) ferromagnetic point. Accordingly, an essential singularity results from a catastrophe point, in a similar way to the Kosterlitz-Thouless transitions [30]. Second, the phase transition from the ferromagnetic phase to the dimerized phase is direct, consistent with Ref. [2]. The transition point, located at the SU(3) ferromagnetic point, features scale invariant ground states, with the fractal dimension being equal to 2. Indeed, the SU(2) ferromagnetic states are smoothly embedded into the SU(3) ferromagnetic states from the ferromagnetic phase. In contrast, the essential singularity appears if the SU(3) ferromagnetic point is approached from the dimerized phase. As a consequence, the phase transition is not of the first-order, in contrast to the claim in Ref. [2]. Third, instead of being a crossover [7], the artifacts involve the pseudo first-order phase transition and the pseudo critical points, thus much more complicated than anticipated.

Acknowledgements.- We thank Murray Batchelor, Sam Young Cho, John Ove Fjærestad, Javier Rodríguez-Laguna, Silvia N. Santalla, and Germán Sierra for enlightening discussions. The work is supported by the National Natural Science Foundation of China (Grant No. 11805285).

[1] A. V. Chubukov, Phys. Rev. B **43**, 3337 (1991).
 [2] G. Fáth and J. Sólyom, Phys. Rev. B **51**, 3620 (1995).
 [3] N. Kawashima, Prog. Theor. Phys. Suppl. **145**, 138 (2002).
 [4] B. A. Ivanov and A. K. Kolezhuk, Phys. Rev. B **68**, 052401 (2003).
 [5] K. Buchta, G. Fáth, O. Legeza, and J. Sólyom, Phys. Rev. B **72**, 054433 (2005).
 [6] M. Rizzi, D. Rossini, G. De Chiara, S. Montangero, and R. Fazio, Phys. Rev. Lett. **95**, 240404 (2005).
 [7] A. Läuchli, G. Schmid, and S. Trebst, Phys. Rev. B **74**, 144426 (2006).
 [8] D. Porras, F. Verstraete, and J. I. Cirac, Phys. Rev. B **73**, 014410 (2006).
 [9] O. Romero-Isart, K. Eckert, and A. Sanpera, Phys. Rev. A **75**,

050303 (2007).
 [10] M. V. Rakov and M. Weyrauch, J. Phys. Commun **1**, 015007 (2017).
 [11] J. I. Cirac and G. Sierra, Phys. Rev. B **81**, 104431 (2010); A. E B Nielsen, J. I. Cirac, and G. Sierra, J. Stat. Mech. P11014 (2011).
 [12] G. Fáth and J. Sólyom, Phys. Rev. B **44**, 11836 (1991).
 [13] F. D. M. Haldane, Phys. Lett. A **93**, 464 (1983).
 [14] T. Affeck, T. Kennedy, E. Lieb, and H. Tasaki, Phys. Rev. Lett. **59**, 799 (1987).
 [15] F. Pollmann, A. M. Turner, E. Berg, and M. Oshikawa, Phys. Rev. B **81**, 064439 (2010).
 [16] B. Sutherland, Phys. Rev. B **12**, 3795 (1975).
 [17] L. Takhtajan, Phys. Lett. A **87**, 479 (1982); H. Babujian, Nucl. Phys. B **215**, 317 (1983).
 [18] M. N. Barber and M. T. Batchelor, Phys. Rev. B **40**, 4621 (1989).
 [19] C. D. Batista, G. Ortiz, and J. E. Gubernatis, Phys. Rev. B **65**, 180402 (2002).
 [20] I. Affleck, J. Phys.: Condens. Matter **2**, 405 (1990).
 [21] X.-H. Chen, I. McCulloch, M. T. Batchelor, and H.-Q. Zhou, Phys. Rev. B **102**, 085146 (2020).
 [22] See Supplemental Material at [URL will be inserted by publisher] for the details.
 [23] G. Vidal, Phys. Rev. Lett. **98**, 070201 (2007).
 [24] I. McCulloch, arXiv: 0804.2509 (2008).
 [25] O. A. Castro-Alvaredo and B. Doyon, J. Stat. Mech. P02001 (2011); O. A. Castro-Alvaredo and B. Doyon, Phys. Rev. Lett. **108**, 120401 (2012).
 [26] H. Watanabe and H. Murayama, Phys. Rev. Lett. **108**, 251602 (2012); H. Watanabe and T. Brauner, Phys. Rev. D **84**, 125013 (2011).
 [27] C. H. Bennett, H. J. Bernstein, S. Popescu, and B. Schumacher, Phys. Rev. A **53**, 2046 (1996).
 [28] L. Tagliacozzo, T. R. de Oliveira, S. Iblisdir, and J. I. Latorre, Phys. Rev. B **78**, 024410 (2008).
 [29] F. Pollmann, S. Mukerjee, A. M. Turner, and J. E. Moore, Phys. Rev. Lett. **102**, 255701 (2009).
 [30] H.-L. Wang, J.-H. Zhao, B. Li, and H.-Q. Zhou, J. Stat. Mech. L10001 (2011); H.-L. Wang, A.-M. Chen, B. Li, and H.-Q. Zhou, J. Phys. A: Math. Theor. **45**, 015306 (2012).
 [31] P. Di Francesco, P. Mathieu, and D. Sénéchal, *Conformal Field Theory* (Springer, Berlin, 1997).
 [32] N. D. Mermin and H. Wagner, Phys. Rev. Lett. **17**, 1133 (1966).
 [33] The different values of p and q from the iTEBD and U(1) iDMRG simulations are due to the fact that the constraints of the same value of χ imposed on the infinite MPS representations in the two cases are different.
 [34] Q.-Q. Shi, Y.-W. Dai, H.-Q. Zhou, and I. McCulloch, arXiv: 2201.01071 (2022).
 [35] H.-Q. Zhou and J. P. Barjaktarevič, J. Phys. A: Math. Theor. **41**, 412001 (2008); H.-Q. Zhou, R. Orús, and G. Vidal, Phys. Rev. Lett. **100**, 080601 (2008).
 [36] K. Rodriguez, A. Argüelles, A. K. Kolezhuk, L. Santos, and T. Vekua, Phys. Rev. Lett. **106**, 105302 (2011).

Supplementary Material for “absence of a critical nematic phase in the vicinity of the SU(3) ferromagnetic point for the one-dimensional spin-1 bilinear-biquadratic model”

Yan-Wei Dai,¹ Qian-Qian Shi,¹ Huan-Qiang Zhou,¹ and Ian McCulloch²

¹Centre for Modern Physics, Chongqing University, Chongqing 400044, The People’s Republic of China

²School of Mathematics and Physics, The University of Queensland, St. Lucia, QLD 4072, Australia

PACS numbers:

SI. The two SU(3) symmetries

The Hamiltonian for the one-dimensional spin-1 bilinear-biquadratic model (1) possesses the SU(2) symmetry, with the generators $\sum_j S_j^x$, $\sum_j S_j^y$ and $\sum_j S_j^z$, for a generic value of the parameter ϕ . However, its symmetry is enlarged to SU(3) at four points $\phi = \pi/2$, $3\pi/2$, $\phi = \pi/4$, and $\phi = 5\pi/4$: one is staggered at $\phi = \pi/2$ and $\phi = 3\pi/2$ [1, 2], and the other is uniform at $\phi = \pi/4$ and $\phi = 5\pi/4$ [3].

At $\phi = \pi/2$ and $\phi = 3\pi/2$, the staggered SU(3) symmetry is realized in terms of the spin-1 operators: $J_\alpha = \sum_j J_\alpha^j$ ($\alpha = 1, 2, \dots, 8$), with $J_1 = 1/2 \sum_j S_j^x$, $J_2 = 1/2 \sum_j S_j^y$, $J_3 = 1/2 \sum_j S_j^z$, $J_4 = 1 - 3/2 \sum_j (-1)^{j+1} (S_j^z)^2$, $J_5 = 1/2 \sum_j (-1)^{j+1} ((S_j^x)^2 - (S_j^y)^2)$, $J_6 = 1/2 \sum_j (-1)^{j+1} (S_j^y S_j^z + S_j^z S_j^y)$, $J_7 = 1/2 \sum_j (-1)^{j+1} (S_j^z S_j^x + S_j^x S_j^z)$ and $J_8 = 1/2 \sum_j (-1)^{j+1} (S_j^x S_j^y + S_j^y S_j^x)$.

At $\phi = \pi/4$ and $\phi = 5\pi/4$, the uniform SU(3) symmetry is realized in terms of the spin-1 operators: $K_\alpha = \sum_j K_\alpha^j$ ($\alpha = 1, 2, \dots, 8$), with $K_1 = 1/2 \sum_j S_j^x$, $K_2 = 1/2 \sum_j S_j^y$, $K_3 = 1/2 \sum_j S_j^z$, $K_4 = 1 - 3/2 \sum_j (S_j^z)^2$, $K_5 = 1/2 \sum_j ((S_j^x)^2 - (S_j^y)^2)$, $K_6 = 1/2 \sum_j (S_j^y S_j^z + S_j^z S_j^y)$, $K_7 = 1/2 \sum_j (S_j^z S_j^x + S_j^x S_j^z)$ and $K_8 = 1/2 \sum_j (S_j^x S_j^y + S_j^y S_j^x)$.

SII. The central charge c in the pseudo critical regime and at the pseudo critical points

The entanglement entropy is defined as $S = -Tr \rho \ln \rho$, which may be exploited to quantify the bipartite entanglement [4]. In our case, the density matrix $\rho = |\varphi\rangle\langle\varphi|$ is generated from the ground state wave function $|\varphi\rangle$, in the infinite MPS representation from the tensor network simulations. For our purpose, we consider the entanglement entropy for a semi-infinite chain, which may be rewritten as

$$S(\phi, \chi) = - \sum_{\mu} \lambda_{\mu}^2(\phi, \chi) \ln \lambda_{\mu}^2(\phi, \chi), \quad (S1)$$

where $\lambda_{\mu}^2(\phi, \chi)$ is the Schmidt decomposition coefficients. The finite-entanglement scaling (2) [5, 6] is performed for the $S(\phi, \chi)$ to extract the central charge c in the pseudo critical regime as well as from the pseudo critical points $\phi_c(\chi)$. Note that the correlation length ξ is defined in terms of the ratio between the largest eigenvalue ε_0 and the second largest eigenvalue ε_1 of the transfer matrix: $\xi = 1/|\ln |\varepsilon_0/\varepsilon_1||$.

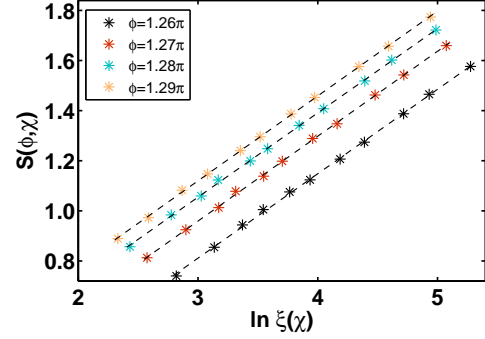


FIG. S1: (color online) The iTEBD simulation for the finite-entanglement scaling: $S(\phi, \chi)$ versus $\ln \xi(\chi)$, in the pseudo critical regime. Here, $\phi = 1.26\pi, 1.27\pi, 1.28\pi$ and 1.29π , and the bond dimension χ ranges from 16 to 300. The central charge c is extracted to be $c = 2$ in the pseudo critical regime.

TABLE I: The central charge c is extracted to be $c = 2$ in the pseudo critical regime from the iTEBD simulation. Here, $\phi = 1.26\pi, 1.27\pi, 1.28\pi$ and 1.29π .

ϕ	1.26π	1.27π	1.28π	1.29π
c	2.0214	2.0322	2.0184	2.0334

1. The central charge c from the iTEBD simulation

For our purpose, we focus on the region $(1.25\pi, 1.5\pi]$ of the parameter ϕ and exploit the iTEBD to simulate the model (1). As a result, a pseudo critical point $\phi_c(\chi)$ is detected from the iTEBD simulation for each value of the bond dimension χ . Therefore, the region is separated into the pseudo critical regime and the dimerized regime.

In order to characterize the pseudo critical regime, the finite-entanglement scaling for the entanglement entropy $S(\phi, \chi)$ is performed for various values of ϕ in the pseudo critical regime, with the bond dimension χ ranging from 16 to 300. Here, we have randomly chosen $\phi = 1.26\pi, 1.27\pi, 1.28\pi$ and 1.29π , which are located in the pseudo critical regime. In Fig. S1, the best linear fit is exploited to estimate the central charge c , which is listed in Table I. The iTEBD simulation yields that the central charge is $c = 2$, with a relative error being less than 2% in the pseudo critical regime.

In addition, the central charge c is extracted by performing

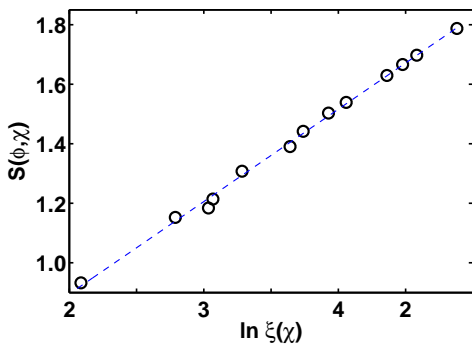


FIG. S2: (color online) The iTEBD simulation for the finite-entanglement scaling: $S(\phi, \chi)$ versus $\ln \xi(\chi)$, at the pseudo critical points $\phi_c(\chi)$. The bond dimension χ ranges from 10 to 200. The central charge c is extracted to be $c = 1.8624$, close to the expected value $c = 2$, with a relative error being less than 7%.

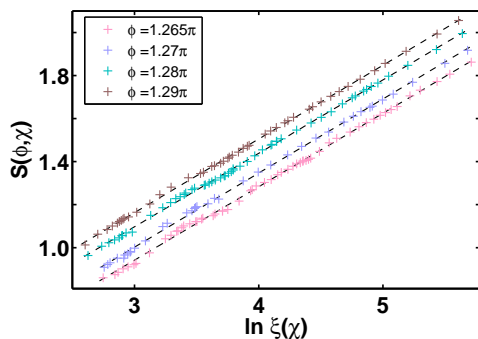


FIG. S3: (color online) The U(1) iDMRG simulation for the finite-entanglement scaling: $S(\phi, \chi)$ versus $\ln \xi(\chi)$, with the bond dimension χ ranging from 30 to 1000. Here, $\phi = 1.265\pi, 1.27\pi, 1.28\pi$ and 1.29π . The central charge c is extracted to be $c = 2$ in the pseudo critical regime.

the finite-entanglement scaling from the pseudo critical points $\phi_c(\chi)$. In Fig. S2, we plot the entanglement entropy $S(\phi, \chi)$ versus $\ln \xi(\chi)$, with the bond dimension ranging from 10 to 200. The best linear fit is exploited to estimate the central charge $c = 1.8624$, with a relative error being less than 7%, compared to the expected value $c = 2$. Here, we stress that the less accurate central charge c extracted from the pseudo critical points results from an error in determining the locations of the pseudo critical points $\phi_c(\chi)$, due to the high computational costs involved in the iTEBD simulation, which may be significantly improved if more trials are implemented.

TABLE II: The central charge c is extracted to be $c = 2$ in the pseudo critical regime from the U(1) iDMRG simulation. Here, $\phi = 1.265\pi, 1.27\pi, 1.28\pi$ and 1.29π .

ϕ	1.265π	1.27π	1.28π	1.29π
c	2.0478	2.0664	2.0478	2.055

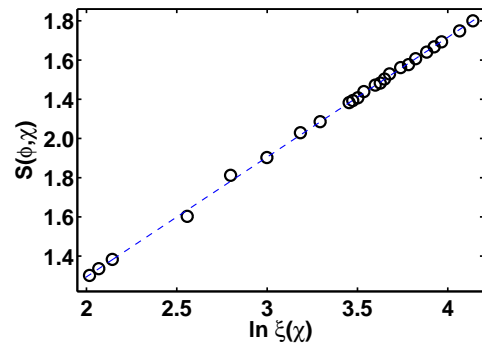


FIG. S4: (color online) The U(1) iDMRG simulation for the finite-entanglement scaling: $S(\phi, \chi)$ versus $\ln \xi(\chi)$, at the pseudo critical points $\phi_c(\chi)$. The bond dimension χ ranges from 60 to 600. The central charge c is extracted to be $c = 1.833$, with a relative error being less than 8.4%, compared to the expected value $c = 2$.

2. The central charge c from the U(1) iDMRG simulation

The U(1) iDMRG simulation is performed for the model (1) in the region $(1.25\pi, 1.4\pi]$. Two pseudo phase transition points are detected from the U(1) iDMRG simulation for each value of the bond dimension χ : one is a pseudo first-order phase transition point $\phi_f(\chi)$, and the other is a pseudo critical point $\phi_c(\chi)$. The latter also occurs in the iTEBD simulation, though the former does not. The two pseudo phase transition points separate the region into three regimes: the pseudo fractal regime, the pseudo critical regime and the dimerized regime.

The finite-entanglement scaling is performed for the entanglement entropy $S(\phi, \chi)$, with $\phi = 1.265\pi, 1.27\pi, 1.28\pi$ and 1.29π , which are located in the pseudo critical regime from the U(1) iDMRG simulation. In Fig. S3, we plot the entanglement entropy $S(\phi, \chi)$ versus $\ln \xi(\chi)$, with the bond dimension χ ranging from 30 to 1000. The best linear fit is exploited to estimate the central charge c , which is listed in Table II. The U(1) iDMRG simulation yields that the central charge is $c = 2$, with a relative error being less than 4% in the pseudo critical regime, consistent with the iTEBD simulation.

The central charge c is also extracted by performing the finite-entanglement scaling from the pseudo critical points $\phi_c(\chi)$ between the pseudo critical regime and the dimerized regime, determined from the U(1) iDMRG simulation. In Fig. S4, the best linear fit is exploited to estimate the central charge $c = 1.833$, with the bond dimension χ ranging from 60 to 600. As a result, the central charge c is close to the expected value $c = 2$, with a relative error being less than 8.4%. Similar to the iTEBD simulation, this may be significantly improved if more trials are implemented.

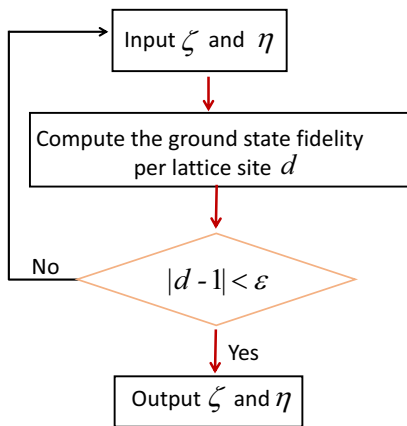


FIG. S5: (color online) A flow chart to determine the directional vector \vec{n} for a ground state wave function generated from the iTEBD and U(1) iDMRG simulations. Here, ε denotes a preset error.

III. Pseudo SSB in the pseudo critical regime: the iTEBD and the U(1) iDMRG simulations

To set the stage, we introduce a few notations. For a directional vector $\vec{n} = (\cos \zeta \cos \eta, \cos \zeta \sin \eta, \sin \zeta)$, the spin component $S_j^{\vec{n}}$ along the directional vector \vec{n} takes the form: $S_j^{\vec{n}} = \cos \zeta \cos \eta S_j^x + \cos \zeta \sin \eta S_j^y + \sin \zeta S_j^z$. Our task is to determine the directional vector \vec{n} , along which the global spin \mathbf{S} is spontaneously polarized for a given ground state wave function generated from the iTEBD and the U(1) iDMRG algorithms. For this purpose, a subroutine is developed to determine the directional vector \vec{n} for spontaneous polarization as a result of pseudo SSB in the pseudo critical regime, with flow chart being shown in Fig. S5.

For a given $\zeta \in [0, \pi]$ and $\eta \in [0, 2\pi]$, we compute the ground state fidelity per lattice site d [12] (also cf. Eq.(S2) below in Sec. SV) between $|\psi\rangle$ and $U|\psi\rangle$. Here, $|\psi\rangle$ is a ground state wave function generated from the iTEBD and the U(1) iDMRG algorithms, and $U = \exp(i\omega S^{\vec{n}})$, with ω being a real number. The idea is to optimize the ground state fidelity per lattice site d , when ζ and η are varied.

The procedure is as follows. (i) Input an initial value of ζ and η , ζ is varied from 0 to π , and η is varied from 0 to 2π , respectively, with the step size being 0.01. (ii) Compute the ground state fidelity per lattice site d . (iii) Compare the ground state fidelity per lattice site d to 1, to see if $|d - 1| > \varepsilon$, with ε being a preset error. If $|d - 1| > \varepsilon$, then return to (i). If $|d - 1| < \varepsilon$, then exit and save the values of ζ and η . In our computation, ω takes an arbitrary value, and the preset error ε is set to be $\varepsilon = 10^{-6}$. Note that the final outcome should not depend on the value of ω .

1. Pseudo SSB in the pseudo critical regime: the iTEBD simulation

The iTEBD algorithm is exploited to generate ground state wave functions for a few selected values of ϕ : $\phi =$

TABLE III: ζ and η for spontaneous polarization in the pseudo critical regime from the iTEBD simulation, with the bond dimension $\chi = 30$. Here, $\phi = 1.26\pi, 1.27\pi, 1.28\pi$ and 1.29π .

ϕ	1.26π	1.27π	1.28π	1.29π
ζ	0.8482	0.7540	0.2827	0.3142
η	0.7540	3.7071	2.1991	2.7332

TABLE IV: ζ and η for spontaneous polarization in the pseudo critical regime from the U(1) iDMRG simulation, with the bond dimension $\chi = 40$. Here, $\phi = 1.268\pi, 1.27\pi, 1.28\pi$ and 1.29π .

ϕ	1.268π	1.27π	1.28π	1.29π
ζ	4.7124	4.7124	4.7124	4.7124
η	0	0	0	0

$1.26\pi, 1.27\pi, 1.28\pi$ and 1.29π , in the pseudo critical region. Here, we choose the bond dimension χ to be $\chi = 30$. The directional vector \vec{n} is determined for spontaneous polarization as a result of pseudo SSB. The results for ζ and η thus yielded are listed in Table III. This indicates that \vec{n} is random, meaning that spontaneous polarization in any direction is possible, consistent with pseudo SSB from SU(2) to U(1). Here, U(1) is generated from $S^{\vec{n}}$.

2. Pseudo SSB in the pseudo critical regime: the U(1) iDMRG simulation

The U(1) iDMRG algorithm is exploited to generate ground state wave functions for a few selected values of ϕ : $\phi = 1.268\pi, 1.27\pi, 1.28\pi$ and 1.29π in the pseudo critical regime, with the bond dimension $\chi = 40$.

The directional vector \vec{n} is determined for spontaneous polarization as a result of pseudo SSB. The results for ζ and η thus yielded are listed in Table IV, meaning that \vec{n} is always along the z axis, as anticipated. This is consistent with pseudo SSB from SU(2) to U(1). Here, U(1) is generated from S^z .

IV. The pseudo local order parameter $\langle O_j(\chi) \rangle$ and the dimerized local order parameter $\langle D_{j,j+1}(\chi) \rangle$

As noted in Ref. [7], the tensor network algorithms in the infinite MPS representation naturally lead to infinitely degenerate ground states in a critical regime, due to the finiteness of the bond dimension. This results in the so-called pseudo continuous SSB [7], with the pseudo symmetry-breaking order being quantified in terms of a pseudo local order parameter $\langle O_j(\chi) \rangle$. Here, we note that the pseudo GMs involved are of type-A, if we adapt the classification of the GMs in

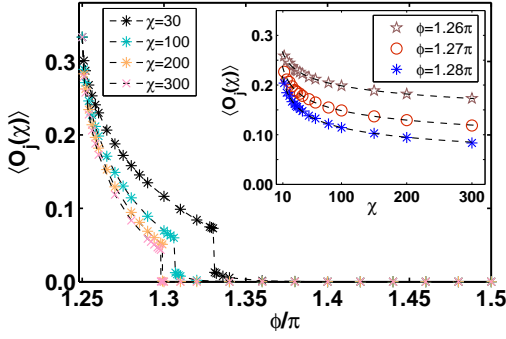


FIG. S6: (color online) Main: the iTEBD simulation results for the pseudo local order parameter $\langle O_j(\chi) \rangle$ as a function of ϕ , with the bond dimension $\chi = 30, 100, 200$ and 300 . The same pseudo critical points $\phi_c(\chi)$ are detected as those from the entanglement entropy $S(\phi, \chi)$. Inset: the pseudo local order parameter $\langle O_j(\chi) \rangle$ may be scaled down to zero, when the bond dimension χ tends to infinity, in the pseudo critical phase. Here, the fitting function is $\langle O_j(\chi) \rangle = s\chi^t$, with $s = 0.3528, 0.3704$ and 0.3970 and $t = -0.1249, -0.1985$ and -0.2701 , for $\phi = 1.26\pi, 1.27\pi$ and 1.28π , respectively.

effective field theories [8] to the pseudo GMs arising from the finiteness of the bond dimension in the tensor network simulations. In order to keep consistency with the Mermin-Wagner theorem [9], $\langle O_j(\chi) \rangle$ must be scaled down to zero, when the bond dimension χ tends to infinity. Here, by the Mermin-Wagner theorem we mean a statement that no continuous symmetry group is spontaneously broken in one dimensional quantum many-body systems, if the GMs involved are of type-A. As a consequence, the Mermin-Wagner theorem does not rule out the possibility for continuous SSB in one dimensional many-body quantum systems, if the GMs involved are of type-B [8, 10].

Physically, the finiteness of the bond dimension χ in the implementation of the tensor network algorithms in the infinite MPS representation amounts to introducing extra long-range interactions into the model Hamiltonian, which turns a quantum many-body system in one spatial dimension into one in higher than one spatial dimensions, if one insists to consider only the short-range interactions. This makes it possible for continuous SSB with the pseudo GMs of type-A to occur in numerical simulations of one dimensional quantum many-body systems, which constitutes the origin of a pseudo critical regime.

For the model (1), a pseudo critical regime with the central charge $c = 2$ does occur, as a result of pseudo SSB from $SU(2)$ to $U(1)$, which has been confirmed in Sec. SIII. Given the directional vector \vec{n} for spontaneous polarization is random, the three spin components S^x, S^y , and S^z are broken, but leaving $S^{\vec{n}}$ invariant. That is, $\langle S_j^x \rangle = 0, \langle S_j^y \rangle = 0$, and $\langle S_j^z \rangle = 0$ in the iTEBD simulation. As it turns out, the remaining five local components of the eight generators, K_α^j ($\alpha = 1, \dots, 8$), of the $SU(3)$ group, discussed in Sec. SI, yield non-zero expectation values, thus constituting a vector which acts as a pseudo local order parameter. However, it is convenient to choose a pseudo local order parameter, which does not depend on an initial

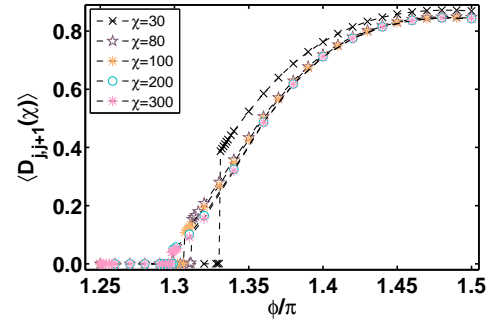


FIG. S7: (color online) The iTEBD simulation results for the dimerized local order parameter $\langle D_{j,j+1}(\chi) \rangle$ as a function of ϕ , with the bond dimension $\chi = 30, 80, 100, 200$ and 300 . The same pseudo critical points $\phi_c(\chi)$ are detected as those from the entanglement entropy $S(\phi, \chi)$.

state. For this purpose, we adopt $\langle O_j(\chi) \rangle$, defined in (3), as the pseudo local order parameter. Note that $\langle K_1^j \rangle, \langle K_2^j \rangle$, and $\langle K_3^j \rangle$, which are essentially $\langle S_j^x \rangle, \langle S_j^y \rangle$, and $\langle S_j^z \rangle$, are included in (3), since they are all zero. Indeed, the (Cartan) metric tensor $g_{\alpha\beta}$ is defined as $g_{\alpha\beta} = \sum_{\delta, \epsilon=1}^8 \gamma_{\alpha\delta\epsilon} \gamma_{\beta\delta\epsilon}$, with $\gamma_{\alpha\beta\epsilon}$ being the structural constants of the $SU(3)$ group: $[K_\alpha, K_\beta] = i \sum_{\delta=1}^8 \gamma_{\alpha\beta\delta} K_\delta$. Alternatively, the metric tensor $g_{\alpha\beta}$ may be defined through the Killing form as $g_{\alpha\beta} = B(K_\alpha, K_\beta)$ [11]. The independence of $\langle O_j(\chi) \rangle$ on an initial state is confirmed.

In addition, the dimerized local order parameter $\langle D_{j,j+1} \rangle$ is introduced to characterize the dimerized phase. The dimerized local order parameter $\langle D_{j,j+1}(\chi) \rangle$, together with the pseudo local order parameter $\langle O_j(\chi) \rangle$, provide other means to confirm the pseudo phase transition points detected from the entanglement entropy $S(\phi, \chi)$.

1. The pseudo local order parameter $\langle O_j(\chi) \rangle$ and the dimerized local order parameter $\langle D_{j,j+1}(\chi) \rangle$: the iTEBD simulation

In Fig. S6, we plot the pseudo local order parameter $\langle O_j(\chi) \rangle$ as a function of ϕ . From this we see the same pseudo critical points $\phi_c(\chi)$ as those detected from the entanglement entropy $S(\phi, \chi)$. Specifically, the pseudo critical points $\phi_c(\chi)$ between the pseudo critical regime and the dimerized regime are located at $\phi_c(\chi) = 1.33\pi, 1.306\pi, 1.299\pi$ and 1.298π for the bond dimension $\chi = 30, 100, 200$ and 300 , respectively.

We remark that the pseudo local order parameter $\langle O_j(\chi) \rangle$ is nonzero in the pseudo critical phase, due to the finiteness of the bond dimension χ , which is scaled down to zero, as the bond dimension χ tends to infinity. This is shown in Fig. S6, as required to keep consistency with the Mermin-Wagner theorem [9].

We plot the dimerized local order parameter $\langle D_{j,j+1}(\chi) \rangle$ in Fig. S7, as a function of ϕ in the region $(1.25\pi, 1.5\pi]$, with the bond dimension $\chi = 30, 80, 100, 200$ and 300 . Note that the dimerized local order parameter $\langle D_{j,j+1}(\chi) \rangle$ tends to be saturated, as the bond dimension χ increases. The same pseudo

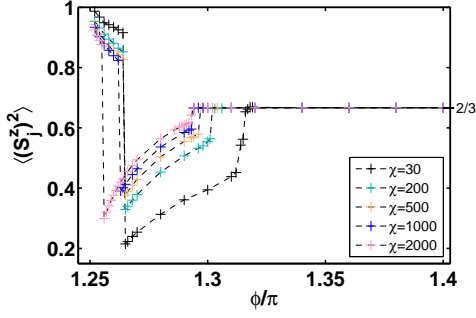


FIG. S8: (color online) The U(1) iDMRG simulation results for the pseudo local order parameter $\langle\langle S_j^z \rangle\rangle^2$ as a function of ϕ , with the bond dimension $\chi = 30, 200, 500, 1000$ and 2000 . The same pseudo first-order transition points $\phi_f(\chi)$ and pseudo critical points $\phi_c(\chi)$ are detected as those from the entanglement entropy $S(\phi, \chi)$.

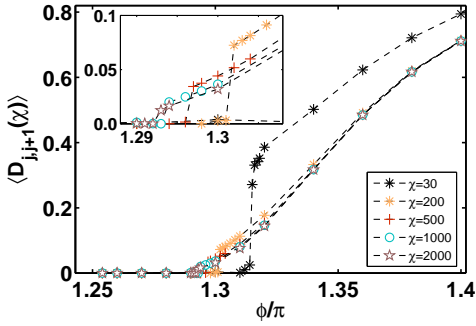


FIG. S9: (color online) The U(1) iDMRG simulation results for the dimerized local order parameter $\langle D_{j,j+1}(\chi) \rangle$ as a function of ϕ . The inset shows a magnification of the dimerized order parameter in the region $(1.288\pi, 1.305\pi)$, with the bond dimension $\chi = 200, 500, 1000$ and 2000 . The same pseudo critical points $\phi_c(\chi)$ are detected as those from the entanglement entropy $S(\phi, \chi)$.

critical points $\phi_c(\chi)$ are detected as those from the pseudo local order parameter $\langle O_j(\chi) \rangle$ and the entanglement entropy $S(\phi, \chi)$.

2. The pseudo local order parameter $\langle O_j(\chi) \rangle$ and the dimerized local order parameter $\langle D_{j,j+1}(\chi) \rangle$: the U(1) iDMRG simulation

In the U(1) iDMRG simulation, both the pseudo fractal regime and the pseudo critical regime may be characterized in terms of the pseudo order parameter $\langle O_j(\chi) \rangle$. Note that, since the z -component of the total spin is preserved to be zero, only $K_4^j = I - 3/2(S_j^z)^2$ yields a non-zero expectation value. Therefore, the pseudo local order parameter $\langle O_j(\chi) \rangle$, as defined in (3), is reduced to $\langle O_j \rangle = 3 - 9/2\langle\langle S_j^z \rangle\rangle^2$. Therefore, $\langle O_j(\chi) \rangle$ may be replaced by the pseudo local order parameter $\langle\langle S_j^z \rangle\rangle^2$. In Fig.S8, we plot the pseudo local order parameter $\langle\langle S_j^z \rangle\rangle^2$ as a function of ϕ , for the bond dimension $\chi = 30, 200, 500, 1000$ and 2000 , respectively. From this we observe that two pseudo phase transition points are detected from the pseudo local order parameter $\langle\langle S_j^z \rangle\rangle^2$, con-

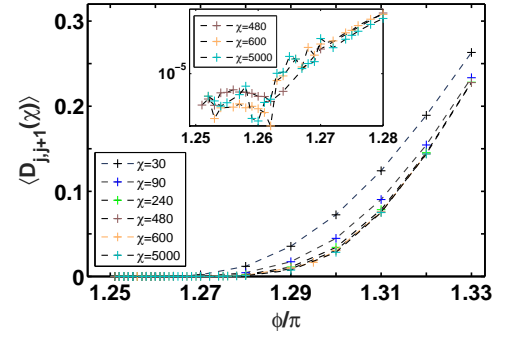


FIG. S10: The SU(2) iDMRG simulation results for the dimerized local order parameter $\langle D_{j,j+1}(\chi) \rangle$ as a function of ϕ . The inset shows a magnification of the dimerized order parameter in the region $(1.251\pi, 1.28\pi)$, with the bond dimension $\chi = 480, 600$ and 5000 .

sistent with those from the entanglement entropy $S(\phi, \chi)$. Specifically, the pseudo first-order phase transition points $\phi_f(\chi)$ and the pseudo critical points $\phi_c(\chi)$ are located at $\phi_f(\chi) = 1.265\pi, 1.265\pi, 1.265\pi, 1.263\pi, 1.256\pi$ and $\phi_c(\chi) = 1.315\pi, 1.301\pi, 1.296\pi, 1.293\pi, 1.292\pi$, with the bond dimension $\chi = 30, 200, 500, 1000$ and 2000 , respectively. In the pseudo fractal regime, we have $\langle\langle S_j^z \rangle\rangle^2 > 2/3$. Therefore, SU(2) is spontaneously broken to U(1), with two broken generators yielding one pseudo GM of type-B. This implies that the fractal dimension d_f , which measures the number of the pseudo GMs of type-B [10], is equal to 1. In contrast, in the pseudo critical regime, we have $\langle\langle S_j^z \rangle\rangle^2 < 2/3$. Therefore, SU(2) is spontaneously broken to U(1), with two broken generators yielding two pseudo GMs of type-A. This implies that the central charge c , which measures the number of gapless excitations, equal to 2, since the two pseudo GMs of type-A evolves into two gapless excitations, as the bond dimension χ tends to infinity. Note that $\langle\langle S_j^z \rangle\rangle^2$ approaches $2/3$ to recover the SU(2) symmetry, as the bond dimension χ increases.

In addition, the dimerized local order parameter is plotted in Fig. S9 as a function of ϕ , with $\chi = 200, 500, 1000$ and 2000 , from the U(1) iDMRG simulation. The inset shows a magnification of the dimerized local order parameter $\langle D_{j,j+1}(\chi) \rangle$ in the region $(1.288\pi, 1.305\pi)$, with $\chi = 200, 500, 1000$ and 2000 . As a result, the pseudo critical points $\phi_c(\chi)$ between the dimerized regime and the pseudo critical regime are detected, consistent with those from the pseudo local order parameter $\langle\langle S_j^z \rangle\rangle^2$ as well as the entanglement entropy $S(\phi, \chi)$.

3. The dimerized local order parameter $\langle D_{j,j+1}(\chi) \rangle$ from the SU(2) iDMRG simulation

The SU(2) iDMRG simulation is performed for the model (1) in the region $(1.251\pi, 1.33\pi)$. In Fig.S10, we plot the dimerized local order parameters $\langle D_{j,j+1}(\chi) \rangle$ as a function of ϕ , with the bond dimension χ ranging from 30 to 5000. The inset shows a magnification of the dimerized local order parameter $\langle D_{j,j+1}(\chi) \rangle$ as a function of ϕ , with

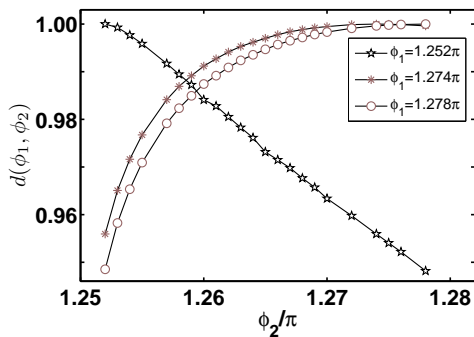


FIG. S11: The SU(2) iDMRG simulation results for the ground state fidelity per lattice site $d(\phi_1, \phi_2)$ as a function of ϕ_2 , with a reference state $|\psi(\phi_1)\rangle$ located at $\phi_1 = 1.252\pi, 1.274\pi$ and 1.278π . Here, the bond dimension χ is 5000.

the bond dimension $\chi = 480, 600$ and 5000 , in the region $(1.251\pi, 1.28\pi]$. Fig. S10 indicates that the dimerized order parameter $\langle D_{j,j+1}(\chi) \rangle$ decreases, as $\phi = 5\pi/4$ is approached. However, we remark that the accuracies get worse, and so the simulation results become less reliable, when ϕ gets close to $5\pi/4$.

SV. Ground state fidelity per lattice site $d(\phi_1, \phi_2)$ from the SU(2) iDMRG simulation

For two given ground states $|\psi(\phi_1)\rangle$ and $|\psi(\phi_2)\rangle$, the ground state fidelity $F = \langle \psi(\phi_1) | \psi(\phi_2) \rangle$ asymptotically scales as $F(\phi_1, \phi_2) \sim d(\phi_1, \phi_2)^L$, with L being the system size. Here, $d(\phi_1, \phi_2)$ is the ground state fidelity per lattice site, which is well-defined in the thermodynamic limit [12]:

$$\ln d(\phi_1, \phi_2) \equiv \lim_{L \rightarrow \infty} \frac{\ln F(\phi_1, \phi_2)}{L}. \quad (\text{S2})$$

As a convention, we choose $|\psi(\phi_1)\rangle$ as a reference state, and regard $d(\phi_1, \phi_2)$ as a function of ϕ_2 for fixed ϕ_1 .

In Fig. S11, we plot the ground state fidelity per lattice site $d(\phi_1, \phi_2)$ as a function of ϕ_2 , with $\chi = 5000$, in the region $(1.251\pi, 1.28\pi)$. Here, the reference state $|\psi(\phi_1)\rangle$ has been chosen to be located at $\phi_1 = 1.252\pi, 1.274\pi$ and 1.278π , respectively. No pinch point is observed, indicating that there is no phase transition in the region $(1.251\pi, 1.28\pi)$.

SVI. Two scenarios arising from the tensor network simulations

For each value of the bond dimension χ , the iTEBD simulation yields a pseudo critical point $\phi_c(\chi)$, which may be detected by means of the entanglement entropy $S(\phi, \chi)$, the pseudo local order parameter $\langle O_j(\chi) \rangle$ and the dimerized local order parameter $\langle D_{j,j+1}(\chi) \rangle$, as shown in Fig. 2, Fig. S6 and Fig. S7, respectively. The central charge c is estimated to be $c = 2$, with a reasonable relative error, in the pseudo critical regime. One may perform an extrapolation of the pseudo

critical point $\phi_c(\chi)$ to see if they terminate at the SU(3) ferromagnetic point. In Fig. 2, we have shown that such an extrapolation is possible if one requires the pseudo critical points $\phi_c(\chi)$ to terminate at the SU(3) ferromagnetic point. However, the same extrapolation works well if the pseudo critical points $\phi_c(\chi)$ terminate somewhere next to the SU(3) ferromagnetic point, within the accuracies achievable. Therefore, two scenarios arise: (i) the pseudo critical points $\phi_c(\chi)$ terminate at the SU(3) ferromagnetic point when the bond dimension χ tends to infinity; (ii) the pseudo critical points $\phi_c(\chi)$ terminate at a point ϕ_c away from the SU(3) ferromagnetic point. Here, ϕ_c is defined to be a point, to which $\phi_c(\chi)$ approaches, when the bond dimension χ tends to infinity.

The two scenarios from the iTEBD simulation have been sketched in Fig. S12. If the first scenario is valid, then the phase transition from the ferromagnetic phase to the dimerized phase is direct, with the phase transition point located at the SU(3) ferromagnetic point. If the second scenario is valid, then there are two phase transitions from the ferromagnetic phase to the dimerized phase: one is located at the SU(3) ferromagnetic point, and the other is located at the point ϕ_c . Hence, there is a critical nematic phase between the ferromagnetic phase and the dimerized phase.

In the U(1) iDMRG simulation, we target at a ground state with the z -component of the total spin being zero. As shown in Fig. 3, Fig. S8 and Fig. S9, from the entanglement entropy $S(\phi, \chi)$, the pseudo local order parameter $\langle O_j(\chi) \rangle$ and the dimerized local order parameter $\langle D_{j,j+1}(\chi) \rangle$, two phase transitions are detected: one is the pseudo first-order phase transition points $\phi_f(\chi)$, and the other is the pseudo critical points $\phi_c(\chi)$, which have been captured in the iTEBD simulation. The occurrence of the pseudo first-order phase transition points $\phi_f(\chi)$ makes it possible to refine the two scenarios.

For the first scenario, the situation is simple: the pseudo critical regime from the iTEBD simulation is now divided into a pseudo fractal regime and a pseudo critical regime, with the pseudo first-order phase transition separating the two regimes. For the second scenario, one may argue that the pseudo fractal regime should not extend up to a point beyond ϕ_c . That is, ϕ_c must always be in the pseudo critical regime for any value of the bond dimension χ . Actually, performing a truncation by means of the bond dimension χ amounts to introducing an energy scale so that a gapped ground state becomes gapless, as long as the gap is small enough, compared to the energy scale thus introduced. With this in mind, we may expect that a pseudo critical point appears as a shift of the critical point ϕ_c , but both are always in the pseudo critical regime for any value of the bond dimension χ . In addition, the pseudo fractal regime reflects fluctuations from the SU(3) ferromagnetic point. Hence, it has to terminate at a point ϕ_o , which represents the onset of the ferromagnetic fluctuations from the SU(3) ferromagnetic point. Therefore, we have $\phi_o < \phi_c$. This is in accord with our U(1) iDMRG simulation results. In practice, ϕ_o may be replaced by the pseudo first-order phase transition point $\phi_f(\chi)$ corresponding to the smallest value of the bond dimension χ achievable. The two scenarios from the

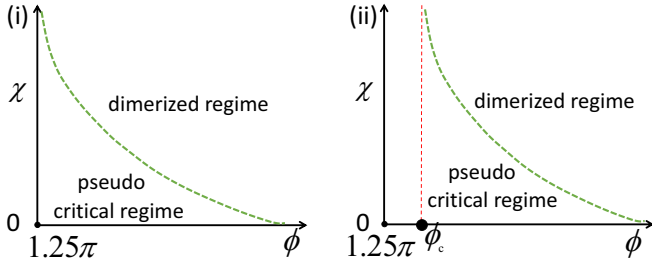


FIG. S12: (color online) A sketch of the two scenarios from the iTEBD simulation for the spin-1 bilinear-biquadratic model in the vicinity of the SU(3) ferromagnetic point.

U(1) iDMRG simulation are sketched in Fig. S13.

We stress that the pseudo first-order phase transition points $\phi_f(\chi)$ must terminate at the SU(3) ferromagnetic point, when the bond dimension χ goes to infinity. This is due to the fact that the pseudo fractal regime, characterized in terms of the fractal dimension $d_f = 1$ (cf. Sec. SVII), results from the proximity effect to the SU(3) ferromagnetic point. Note that the pseudo first-order phase transition points $\phi_f(\chi)$ are quite robust, when the bond dimension χ increases, as seen from Fig. 3 and Fig. S8.

However, the second scenario, sketched in Fig. S13, is ruled out from the SU(2) iDMRG simulation, given no phase transition is detected in the region $\phi_o < \phi < \phi_c$, as shown in Fig. 4, Fig.S10 and Fig.S11, by means of the entanglement entropy $S(\phi, \chi)$, the dimerized local order parameter $\langle D_{i,j+1}(\chi) \rangle$ and the ground state fidelity per lattice site d , respectively. Here, ϕ_o is approximated by the pseudo first-order phase transition point $\phi_f(\chi) = 1.265\pi$ corresponding to the bond dimension $\chi = 30$, and ϕ_c is approximated by the pseudo critical point $\phi_c(\chi) = 1.292\pi$ corresponding to the bond dimension $\chi = 2000$. We remark that the region $1.262\pi < \phi < 1.33\pi$ well covers (ϕ_o, ϕ_c) . As shown in Fig. S10, the dimerized order parameter $\langle D_{i,j+1}(\chi) \rangle$ at the point $\phi_o = 1.265\pi$ from the SU(2) iDMRG simulation is in the order of magnitude 10^{-5} , indicating that the SU(2) iDMRG simulation results are reliable.

Therefore, we conclude that the phase transition from the ferromagnetic phase to the dimerized phase is direct, thus ruling out the existence of a critical nematic phase in the vicinity of the SU(3) ferromagnetic point.

SVII. The fractal dimension d_f in the pseudo fractal regime: the spin-1/2 XXZ model and the spin-1 bilinear-biquadratic model

According to the finite block-size scaling (4) of the entanglement entropy $S(n)$, we are able to extract the fractal dimension d_f from the tensor network simulations for the spin-1 bilinear-biquadratic model in the pseudo fractal regime. We emphasize that such a fractal regime only occurs in the U(1) iDMRG simulation.

For an illustrative purpose, we include our simulation re-

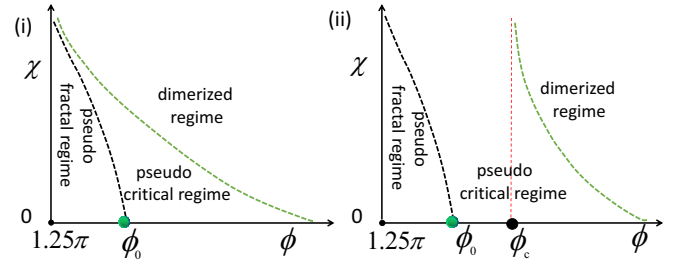


FIG. S13: (color online) A sketch of the two scenarios from the U(1) iDMRG simulation for the spin-1 bilinear-biquadratic model in the vicinity of the SU(3) ferromagnetic point.

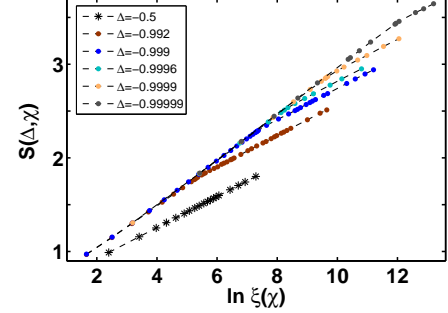


FIG. S14: (color online) The U(1) iDMRG simulation for the finite-entanglement scaling: $S(\Delta, \chi)$ versus $\ln \xi(\chi)$, for the spin-1/2 XXZ model for $\Delta = -0.5, -0.992, -0.999, -0.9996, -0.9999$ and -0.99999 in the vicinity of the SU(2) ferromagnetic point $\Delta = -1$.

sults for the spin-1/2 quantum XXZ model. We remark that it is necessary to develop a subroutine to efficiently calculate the block entanglement entropy $S(n)$. As it turns out, the fractal dimension d_f is equal to the number of the pseudo GMs of type-B, which may be regarded as an adaptation of a general statement [10] about the connection between the fractal dimension and the number of the GMs of type-B to the numerical artifacts.

1. The fractal dimension d_f for the spin-1/2 XXZ model in the vicinity of the ferromagnetic point at $\Delta = -1$

The Hamiltonian for the spin-1/2 anisotropic XXZ model takes the form:

$$H_{\text{XXZ}} = \sum_j [S_j^x S_{j+1}^x + S_j^y S_{j+1}^y + \Delta S_j^z S_{j+1}^z], \quad (\text{S3})$$

where Δ denotes the anisotropic coupling parameter. At $\Delta = -1$, the model possesses the SU(2) symmetry, generated by $\sum_j (-1)^j S_j^x$, $\sum_j (-1)^j S_j^y$ and $\sum_j S_j^z$, which are staggered.

The ground state phase diagram for the spin-1/2 XXZ model involves three distinct phases in the entire parameter region: the ferromagnetic phase ($\Delta < -1$), the critical XY phase ($-1 < \Delta \leq 1$) with the central charge $c = 1$, and the Néel phase ($\Delta > 1$). In the Néel phase, the ground state wave functions are two-fold degenerate, due to SSB of the

TABLE V: The central charge c in the critical XY regime is extracted from the U(1) iDMRG algorithm for the spin-1/2 XXZ model, with the block size n being from 6 to 24. Here, $\Delta = -0.2$ and -0.5 .

	χ	20	40	50	60
$\Delta = -0.2$	c	1.0143	1.0032	1.0026	1.002
$\Delta = -0.5$	c	1.0395	1.0086	1.0056	1.0038

TABLE VI: The fractal dimension d_f in the pseudo fractal regime is extracted from the U(1) iDMRG algorithm for the spin-1/2 XXZ model, with the block size n being from 6 to 24. When $\Delta = -1$ is approached, d_f tends to 1.

	χ	20	40	60	70	78
$\Delta = -0.9999$	d_f	0.799	0.897	0.9406	0.9504	0.953
	χ	20	40	60	80	100
$\Delta = -0.99999$	d_f	0.7998	0.8992	0.9486	0.97	0.972

one-site translational invariance. In the ferromagnetic phase, the ground state wave functions are two-fold degenerate and fully polarized along the z axis. The model is special at the point $\Delta = -1$. In fact, it possesses highly degenerate ground states and is not conformally invariant. A proper description requires to introduce the fractal dimension d_f [13]. Indeed, this description is also necessary to understand the simulation results from the U(1) iDMRG algorithm, if one targets at a ground state with the z -component of the total spin being zero.

In Fig. S14, the finite-entanglement scaling of the entanglement entropy $S(\chi)$ is performed for a few chosen values of Δ . An interesting observation is that, if Δ is far away from the ferromagnetic point at $\Delta = -1$, then all the data falls on a straight line, as the correlation length $\xi(\chi)$ increases with χ . If Δ gets close enough to $\Delta = -1$, the data starts to fall on two segments with a different slope asymptotically (see also Ref. [14]). Physically, this implies a crossover from the pseudo fractal regime to the pseudo critical regime in the vicinity of $\Delta = -1$, as the bond dimension χ increases.

In the critical XY regime, the central charge c may be extracted from the finite block-size scaling $S(n) \sim c/3 \ln n$ [15], which is listed in Table V. In the fractal regime, the fractal dimension d_f may be extracted from the finite block-size scaling of the entanglement entropy $S(n)$ (4), which is listed in Table VI.

A conclusion one may draw from the simulation results is that, as $\Delta = -1$ is approached, the fractal dimension d_f tends to 1, as anticipated. We remark that the U(1) iDMRG algorithm works well even when Δ is so close to -1 , given that it still captures the crossover behavior from the pseudo fractal regime to the pseudo critical regime, as the bond dimension χ increases.

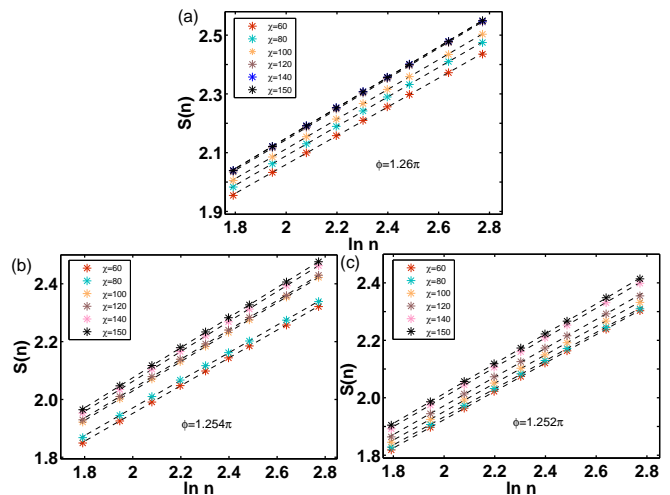


FIG. S15: (color online) The finite block-size scaling of the entanglement entropy $S(n)$ in the pseudo fractal regime for the spin-1 bilinear-biquadratic model, with the bond dimension $\chi = 60, 80, 100, 120, 140$ and 150 , for (a) $\phi = 1.26\pi$; (b) $\phi = 1.254\pi$; and (c) $\phi = 1.252\pi$.

TABLE VII: The fractal dimension d_f in the pseudo fractal regime is extracted from the U(1) iDMRG simulation for the spin-1 bilinear-biquadratic model, with the block size n being from 6 to 16. Here, $\phi = 1.26\pi, 1.254\pi$ and 1.252π .

	χ	60	80	100	120	140	150
$\phi = 1.26\pi$	d_f	0.9802	1.0024	1.0122	1.0384	1.035	1.0364
$\phi = 1.254\pi$	d_f	0.9604	0.9554	1.0178	1.0148	1.0368	1.0418
$\phi = 1.252\pi$	d_f	0.9874	0.9794	0.9898	1.0018	1.0314	1.0404

2. The fractal dimension d_f for the spin-1 bilinear-biquadratic model in the vicinity of the SU(3) ferromagnetic point

The fractal dimension d_f is 2 for the model (1) at the SU(3) ferromagnetic point [10]. We need to extract the fractal dimension d_f from the finite block-size scaling in the pseudo fractal regime in the vicinity of the SU(3) ferromagnetic point for the spin-1 bilinear-biquadratic model. In Fig. S15, the finite block-size scaling of the entanglement entropy $S(n)$ is performed, with the bond dimension $\chi = 60, 80, 100, 120, 140$ and 150 , for (a) $\phi = 1.26\pi$; (b) $\phi = 1.254\pi$; and (c) $\phi = 1.252\pi$, which are located in the pseudo fractal regime. The best linear fit yields that the fractal dimension $d_f = 1$, with n ranging from 6 to 16, with a relative error being less than 5%, as shown in Table VII. Note that the fractal dimension d_f tends to saturation, as the bond dimension χ increases.

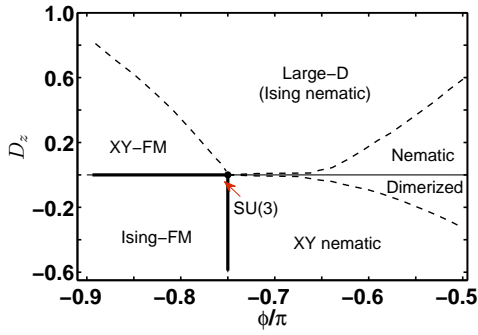


FIG. S16: (color online) A sketch of the ground state phase diagram close to the SU(3) ferromagnetic point for the spin-1 bilinear-biquadratic model (S4) undergoing a quadratic Zeeman effect. This is adapted from Ref. [17]

SVIII. The origins of the pseudo fractal and pseudo critical regimes in the tensor network simulations.

We have demonstrated in Sec. SIII that, in the pseudo critical regime, pseudo SSB from SU(2) symmetry to U(1) occurs. Here, U(1) is generated from $S^{\vec{n}}$, with the directional vector \vec{n} being random and depending on an initial state for a ground state wave function generated from the iTEBD simulation. Therefore, two generators are spontaneously broken, yielding two pseudo GMs of type-A. Therefore, the central charge c takes $c = 2$, given that the central charge c measures the number of gapless low-lying excitations [16]. The same argument also applies to a ground state wave function generated from the U(1) iDMRG simulation, with the only difference being that spontaneous polarization is always along the z -axis in the spin space. This is in sharp contrast to the SU(2) iDMRG simulation, in which the full SU(2) symmetry is implemented so that no pseudo SSB is allowed to occur. Thus, the pseudo critical regime only occurs in the iTEBD simulation and the U(1) iDMRG simulation, but not in the SU(2) iDMRG simulation.

As for the pseudo fractal regime, it only occurs in the U(1) iDMRG simulation, since a ground state with the z -component of the total spin being zero is targeted, ensuring that it is highly entangled so that a scale invariant ground state, characterized in terms of the fractal dimension $d_f = 1$ corresponding to one pseudo GM of type-B, is able to compete with a ground state, characterized in terms of the central charge $c = 2$ corresponding to two pseudo GMs of type-A. In contrast, the z -component of the total spin is not preserved in the iTEBD simulation. Thus, it is impossible to produce such a highly entangled scale invariant ground state. We remark that the fractal dimension d_f is equal to 1 in the pseudo fractal regime, since there is one pseudo GM of type-B as a result of pseudo SSB from SU(2) to U(1). This pseudo GM of type-B evolves into one of the two GMs at the SU(3) ferromagnetic point. Indeed, at this point, two GMs of type-B emerge, as a consequence of SSB from SU(3) to SU(2) \otimes U(1), implying

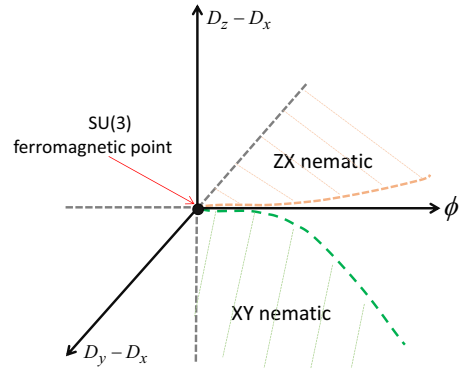


FIG. S17: (color online) A sketch of the two critical nematic phases, close to the SU(3) ferromagnetic point, for the spin-1 bilinear-biquadratic model (S4) undergoing a quadratic Zeeman effect, if one chooses D_x to be a fixed constant. Note that the XY and ZX nematic critical phases are symmetric under the unitary transformation: $S_j^y \leftrightarrow S_j^z$ and $S_j^x \leftrightarrow -S_j^x$. We emphasize that the model possesses a U(1) symmetry only when $D_y = D_x$ or $D_z = D_x$, which is necessary for a critical nematic phase to emerge.

that the fractal dimension d_f is equal to 2. Here, we note that the fractal dimension d_f measures the number of low-lying excitations [10] (also cf. Sec. SVII in SM). As a consequence, one may conclude that the pseudo fractal regime originates from the proximity effect to a highly entangled scale invariant ground state at the SU(3) ferromagnetic point.

The final question we need to address concerns the origin of the pseudo critical regime. Given there is only one phase transition point from the ferromagnetic phase to the dimerized phase located at the SU(3) ferromagnetic point, the model (1) itself does not accommodate any critical nematic phase close to the transition point. Therefore, one may expect that a critical nematic phase exists in the vicinity of the SU(3) ferromagnetic point, if extra interactions are introduced into the model (1). Since $\langle S_j^x \rangle = 0$, $\langle S_j^y \rangle = 0$, and $\langle S_j^z \rangle = 0$, in both the iTEBD simulation and the U(1) simulation, the linear Zeeman effect is not relevant. Instead, we turn to a quadratic Zeeman effect, described by the Hamiltonian:

$$H_{\text{BBXYZ}} = J \sum_j \left[(\cos \phi (\mathbf{S}_j \mathbf{S}_{j+1}) + \sin \phi (\mathbf{S}_j \mathbf{S}_{j+1})^2) \right] + D_x \sum_j (S_j^x)^2 + D_y \sum_j (S_j^y)^2 + D_z \sum_j (S_j^z)^2. \quad (\text{S4})$$

Here, D_x , D_y , and D_z are coupling constants describing a quadratic Zeeman effect. A special case with $D_x = 0$ and $D_y = 0$ has been investigated in Ref. [17]. The ground state phase diagram is sketched in Fig. S16, close to the SU(3) ferromagnetic point. It is found that the XY nematic phase, with the central charge $c = 1$, extends up to the SU(3) ferromagnetic point. In addition, the phase transition from the XY nematic phase to the dimerized phase is of the Kosterlitz-Thouless type. Therefore, for the model (S4), there should be the XY and ZX critical nematic phases, with the central charge $c = 1$, in the vicinity of the SU(3) ferromagnetic point,

due to the local constraints: $(S_j^x)^2 + (S_j^y)^2 + (S_j^z)^2 = 2$, if one chooses D_x to be a fixed constant. The two critical nematic phases are sketched in Fig. S17, which are symmetric under the unitary transformation: $S_j^y \leftrightarrow S_j^z$ and $S_j^x \leftrightarrow -S_j^x$. We emphasize that no other critical regime with the central charge $c = 1$ exists in the vicinity of the SU(3) ferromagnetic point, since the model (S4) possesses a U(1) symmetry only when $D_y = D_x$ or $D_z = D_x$, which is necessary for a critical nematic phase to emerge. This explains why two pseudo GMs of type-A emerge in the iTEBD and U(1) iDMRG simulations, as long as it is close enough to the SU(3) ferromagnetic point. In other words, it is the proximity effect to the two critical nematic phases with $c = 1$, which are infinitesimally close to each other in the vicinity of the SU(3) ferromagnetic point, that constitutes the origin of the pseudo critical regime with $c = 2$ in the iTEBD and U(1) iDMRG simulations. However, the two critical nematic phases with $c = 1$ do not meet each other at the SU(3) ferromagnetic point, though asymptotically close, implying that no SU(2) WZW model with level $k = 4$ exists as a limit of the pseudo critical regime, as the bond dimension χ tends to infinity.

Finally, the proximity effect to the two critical nematic phases with $c = 1$ offers a mechanism to account for the opening of an exponentially decaying small gap, when the SU(3) ferromagnetic point is approached from the dimerized phase. This is due to the facts that the phase transition from the XY/ZX nematic phase to the dimerized phase is of the Kosterlitz-Thouless type, meaning an essential singularity arising from a marginally relevant perturbation at the Kosterlitz-Thouless transition points, and that the two lines of the critical points themselves get close to each other in the vicinity of the SU(3) ferromagnetic point.

We thank Murray Batchelor, Sam Young Cho, John Ove Fjærestad, Javier Rodríguez-Laguna, Silvia N. Santalla, and Germán Sierra for enlightening discussions. The work is supported by the National Natural Science Foundation of China (Grant No. 11805285).

- [2] X.-H. Chen, I. McCulloch, M. T. Batchelor, and H.-Q. Zhou, Phys. Rev. B **102**, 085146 (2020).
- [3] B. Sutherland, Phys. Rev. B **12**, 3795 (1975).
- [4] C. H. Bennett, H. J. Bernstein, S. Popescu, and B. Schumacher, Phys. Rev. A **53**, 2046 (1996).
- [5] L. Tagliacozzo, T. R. de Oliveira, S. Iblisdir, and J. I. Latorre, Phys. Rev. B **78**, 024410 (2008).
- [6] F. Pollmann, S. Mukerjee, A. M. Turner, and J. E. Moore, Phys. Rev. Lett. **102**, 255701 (2009).
- [7] H.-L. Wang, J.-H. Zhao, B. Li, and H.-Q. Zhou, J. Stat. Mech. L10001 (2011); H.-L. Wang, A.-M. Chen, B. Li, and H.-Q. Zhou, J. Phys. A: Math. Theor. **45** 015306 (2012).
- [8] H. Watanabe and H. Murayama, Phys. Rev. Lett. **108**, 251602 (2012); H. Watanabe and T. Brauner, Phys. Rev. D **84**, 125013 (2011).
- [9] N. D. Mermin and H. Wagner, Phys. Rev. Lett. **17**, 1133 (1966).
- [10] Q.-Q. Shi, Y.-W. Dai, H.-Q. Zhou, and I. McCulloch, arXiv: 2201.01071 (2022).
- [11] W. Killing, Math. Ann. **31**, 252 (1888).
- [12] H.-Q. Zhou and J. P. Barjaktarevič, J. Phys. A: Math. Theor. **41**, 412001 (2008); H.-Q. Zhou, R. Orús, and G. Vidal, Phys. Rev. Lett. **100**, 080601 (2008).
- [13] O. A. Castro-Alvaredo and B. Doyon, J. Stat. Mech. 2011 (02): P02001 (2011); O. A. Castro-Alvaredo and B. Doyon, Phys. Rev. Lett. **108**, 120401 (2012).
- [14] P. Chen, Z.-L. Xue, I. P. McCulloch, M.-C. Chung, M. Cazalilla and S. K. Yip, J. Stat. Mech. P10007 (2013). Note that the data these authors presented suffers from a misinterpretation for the correlation length ξ , which results in a marked difference between the data there and in this work for the pseudo fractal regime.
- [15] G. Vidal, J. I. Latorre, E. Rico, and A. Kitaev, Phys. Rev. Lett. **90**, 227902 (2003); P. Calabrese and J. Cardy, J. Stat. Mech. **2004**, P06002 (2004).
- [16] P. Di Francesco, P. Mathieu, and D. Sénéchal, *Conformal Field Theory* (Springer, Berlin, 1997).
- [17] K. Rodriguez, A. Argüelles, A. K. Kolezhuk, L. Santos, and T. Vekua, Phys. Rev. Lett. **106**, 105302 (2011); G. De Chiara, M. Lewenstein, and A. Sanpera, Phys. Rev. B **84**, 054451 (2011).

[1] I. Affleck, J. Phys.: Condens. Matter **2**, 405 (1990).